Applied Catalysis B: Environmental 165 (2015) 57–62

Contents lists available at ScienceDirect

Applied Catalysis B: Environmental

journal homepage: www.elsevier.com/locate/apcatb

Synergistic catalysis of AgPd@ZIF-8 on dehydrogenation of formic acid

Hongmei Dai[a,1], Bingquan Xia[a,1], Lan Wen[a], Cheng Du[a], Jun Su[c], Wei Luo[a,b,*], Gongzhen Cheng[a]

[a] College of Chemistry and Molecular Sciences, Wuhan University, Wuhan, Hubei 430072, PR China
[b] Suzhou Institute of Wuhan University, Suzhou, Jiangsu, 215123, PR China
[c] Wuhan National Laboratory for Optoelectronics, Huazhong University of Science and Technology, Wuhan, Hubei, 430073, PR China

ARTICLE INFO

Article history:
Received 25 July 2014
Received in revised form
22 September 2014
Accepted 25 September 2014
Available online 5 October 2014

Keywords:
ZIF-8
Palladium
Silver
Formic acid
Hydrogen storage

ABSTRACT

Highly dispersed bimetallic AgPd nanoparticles with different composition have been successfully deposited on the metal-organic frameworks (ZIF-8) by using a simple liquid impregnation method. The resultant catalysts are composition dependent toward dehydrogenation of formic acid, while $Ag_{18}Pd_{82}$@ZIF-8 exhibits exceedingly high catalytic activity, with the turnover frequency (TOF) value of 580 h^{-1}, and 100% hydrogen selectivity at 80 °C.

© 2014 Elsevier B.V. All rights reserved.

1. Introduction

In recent years, due to the high specific surface area and tunable pore size, porous metal-organic frameworks (MOFs) have attracted growing attention in the application of drug delivery [1,2], gas sorption and storage [3–5], molecular separation [6–8], and heterogeneous catalysis [9,10]. Given the similarity to zeolites, loading of metal nanoparticles (NPs) inside the porous of MOFs could control the size of NPs, restrain the aggregation of the metal NPs, and further affect the catalytic activity and recyclability of the catalysts [11–13]. So far, there have been limited examples concerning monometallic NPs@MOF, and only few reports about MOF supported bimetallic NPs with full characterization as catalysts for heterogeneous reaction, since the metal alloying could promote the catalytic activity and selectivity of their monometallic counterparts [14].

On the other hand, the safe and efficient storage of hydrogen is still the key issue for the "hydrogen economy" [15–17]. Various hydrogen storage approaches are currently being investigated, including metal hydrides [18], sorbent materials [19], and chemical hydride systems [20]. Notably, formic acid (HCOOH, FA) as a liquid hydrogen fuel possesses the potential advantages of taking the current liquid-based distribution infrastructure, making it more competitive compared with the widely-studied solid chemical hydrogen storage materials such as sodium borohydride ($NaBH_4$) and ammonia borane (NH_3BH_3) derivatives. Moreover, formic acid as an easy recharging fuel, is nontoxic and highly stable with a high H_2 content (4.4%) at room temperature, making it safe and convenient H_2 carrier for portable hydrogen storage application [15]. The decomposition of formic acid follows two principal pathways [21–23], reaction (2) is the undesirable pathway as

$$HCOOH(l) \rightarrow CO_2(g) + H_2(g) \quad \Delta G_{298} = -48.8\ kJ\ mol^{-1} \qquad (1)$$

$$HCOOH(l) \rightarrow H_2O(l) + CO(g) \quad \Delta G_{298} = -28.5\ kJ\ mol^{-1} \qquad (2)$$

CO is toxic to fuel cells catalysts [24]. Recently, Pd-based multimetallic NPs including AgPd [25,26], NiAgPd [27], AuPd [28], CoAuPd [29], Ag@Pd [30], Au@Pd [31], monodisperse AgPd [32], and AuPd [33], supported on carbon based materials have been development as efficient catalysts for catalytic dehydrogenation of formic acid. However, to the best of our knowledge, there is only one report about MOFs supported AuPd NPs for catalytic dehydrogenation of formic acid [34]. The authors studied the synergistic effect of different MOFs (derivatives of MIL-101) on the catalytic activity of AuPd clusters.

* Corresponding author at: College of Chemistry and Molecular Sciences, Wuhan University, Wuhan, Hubei 430072, PR China. Tel.: +86 2768752366.
E-mail address: wluo@whu.edu.cn (W. Luo).
[1] These authors contributed equally to this work.

http://dx.doi.org/10.1016/j.apcatb.2014.09.065
0926-3373/© 2014 Elsevier B.V. All rights reserved.

To screen out new efficient catalysts, using a more cost effective metal Ag instead of Au, herein, we reported the generation of highly dispersed AgPd NPs immobilized on ZIF-8 with different composition, studied the synergistic effect of metal compositions in MOFs for the catalytic dehydrogenation of formic acid. The ZIF-8 framework ($Zn(MeIM)_2$, MeIM = 2-methylimidazole), one of the predominant MOFs, was used as an ideal support for catalysts [35–38], because of its intersecting three-dimensional structural feature, high thermal and chemical stability, and large surface area [39,40]. As expected, the resultant $Ag_{18}Pd_{82}$@ZIF-8 exhibits excellent catalytic activity with the turnover frequency (TOF) value of 580 h^{-1}, and 100% hydrogen selectivity toward dehydrogenation of FA at 80 °C.

2. Experimental

2.1. Chemicals and materials

All chemicals were commercial and used without further purification. Zinc nitrate hexahydrate ($Zn(NO_3)_2{\cdot}6H_2O$), Sinopharm Chemical Reagent Co., Ltd. (99.0%), palladium chloride ($PdCl_2$, Great Wall Reagent Co., Ltd., 99%), Silver nitrate ($AgNO_3$, AR), sodium formate (HCOONa, Sinopharm Chemical Reagent Co., Ltd., 99%), formic acid (HCOOH, Sigma–Aldrich 98%), hydrochloric acid (HCl, Sinopharm Chemical Reagent Co., Ltd., 37%), 2-methylimidazole ($Zn(MeIM)_2$, aladdin, 98%), N,N-Dimethylformamide (DMF, Sinopharm Chemical Reagent Co., Ltd., >99.5%), sodium borohydride ($NaBH_4$, Sinopharm Chemical Reagent Co., Ltd., 96%), methanol (CH_3OH, Sinopharm Chemical Reagent Co., Ltd., >99.5%) were used as received. We use ordinary distilled water as the reaction solvent.

2.2. Synthesis of ZIF-8

ZIF-8 was synthesized using the reported procedure [40]. 350 mg of $Zn(NO_3)_2{\cdot}6H_2O$ and 200 mg of 2-methylimidazole were placed in a 20 mL screw-top vial and dissolved in 15 mL of DMF. Three drops of HNO_3 were added to a mixture with a Pasteur pipet, and complete dissolution was achieved by sonication. The vial was capped and placed in an oven at 120 °C for 24 h. ZIF-8 crystals were collected and washed with DMF. The crystals were stored in DMF until needed for experiments.

2.3. Synthesis of H_2PdCl_4

A solution of tetrachloropalladinic acid (0.01 M, H_2PdCl_4) was prepared by mixing 44.5 mg of $PdCl_2$ into 25 mL of HCl (0.02 M) aqueous solution under stirring at room temperature until complete dissolution.

2.4. Preparation of AgPd@ZIF-8

Prior to metal loading, ZIF-8 was pretreated as follows: ZIF-8 were immersed in methanol under ambient conditions for 48 h, evacuated at room temperature for over 10 h, then at 573 K for 2 h to obtain optimally evacuated sample. Typically, for preparation of $Ag_{18}Pd_{82}$@ZIF-8, activated ZIF-8 (100 mg) was added to 5 mL solution of $AgNO_3$ (0.04 mmol) and H_2PdCl_4 (0.16 mmol), stirring for 24 h at 25 °C to impregnate metal salts. The resulting mixture was then reduced by sodium borohydride ($NaBH_4$, 2 mmol) solution with vigorous stirring at 273 K to yield $Ag_{18}Pd_{82}$@ZIF-8. The preparations of $Ag_{25}Pd_{75}$@ZIF-8, $Ag_{48}Pd_{52}$@ZIF-8, $Ag_{58}Pd_{42}$@ZIF-8, $Ag_{76}Pd_{24}$@ZIF-8, Ag@ZIF-8 and Pd@ZIF-8 catalysts were following in similar procedure.

2.5. Preparation of AgPd supported on C, SiO_2 and Al_2O_3

For comparison, $Ag_{18}Pd_{82}$ loaded on C, SiO_2 and Al_2O_3 were prepared. In a typical preparation, 100 mg SiO_2 was added to 5 mL mixture solution containing $AgNO_3$ (0.04 mmol) and H_2PdCl_4 (0.16 mmol). After vigorous stirring at 298 K for 2 h, 2.0 mL aqueous solution of sodium borohydride was added to the mixture and the resulting mixture was stirred at 273 K for 2 h. The final $Ag_{18}Pd_{82}/SiO_2$ was obtained after centrifugation and drying at 373 K.

2.6. H_2 generation from FA/SF over AgPd@ZIF-8

All the catalytic reactions were carried at 353 K under ambient atmosphere. Typically, 2.0 mL aqueous solution containing 100 mg the as-prepared AgPd@ZIF-8 catalyst was kept in a two-neck round-bottle flask. One neck was connected to a pressure-equalization funnel to introduce the mixed solution of formic acid (FA, 3 mmol) and sodium formate (SF, 1 mmol), and the other was connected to a gas burette to monitor the volume of the released gas. The catalytic decomposition reaction begins once the mixed solution of FA/SF was added. In addition, analogous reactions with different molar ratio in FA/SF (18:0, 18:2, 18:3, 18:6, 18:9, 18:12, 0:18) were also applied under ambient atmosphere at 353 K, where FA was kept as 3 mmol.

2.7. H_2 generation from FA/SF over AgPd supported on C, SiO_2 and Al_2O_3

All the catalytic reactions were carried at 353 K under ambient atmosphere. Typically, 2.0 mL aqueous solution containing 100 mg the $Ag_{18}Pd_{82}/SiO_2$ catalyst was kept in a two-neck round-bottle flask. One neck was connected to a pressure-equalization funnel to introduce the mixed solution of formic acid (FA, 3 mmol) and sodium formate (SF, 1 mmol), and the other was connected to a gas burette to monitor the volume of the released gas. The catalytic decomposition reaction begins once the mixed solution of FA/SF was added. The decomposition of FA/SF catalyzed by $Ag_{18}Pd_{82}/C$ and $Ag_{18}Pd_{82}/Al_2O_3$ was followed in the similar method.

2.8. NaOH trap test

To determine CO_2 to H_2 molar ratio in the gas mixture generated during the AgPd@ZIF-8 catalyzed decomposition of FA/SF solution (FA, 3 mmol; SF, 1 mmol), the generated gas was monitored after passing the trap containing 5 M NaOH solution.

2.9. Recyclability test

For recycle stability test, catalytic reactions were repeated five times by adding another equivalent of FA into the mixture after the previous cycle.

2.10. Characterization

The morphologies and sizes of the samples were observed by using a Tecnai G20 U-Twin transmission electron microscope (TEM) equipped with an energy dispersive X-ray detector (EDX) at an acceleration voltage of 200 kV. Powder X-ray diffraction (XRD) patterns were measured by a Bruker D8-Advance X-ray diffractometer using Cu Ka radiation source (λ = 0.154178 nm) with a velocity of 1° min^{-1}. X-ray photoelectron spectroscopy (XPS) measurement was performed with a Kratos XSAM 800 spectrophotometer. The surface area measurements were performed with N_2 adsorption/desorption isotherms at liquid nitrogen temperature (77 K) after dehydration under vacuum at 373 K for 12 h using

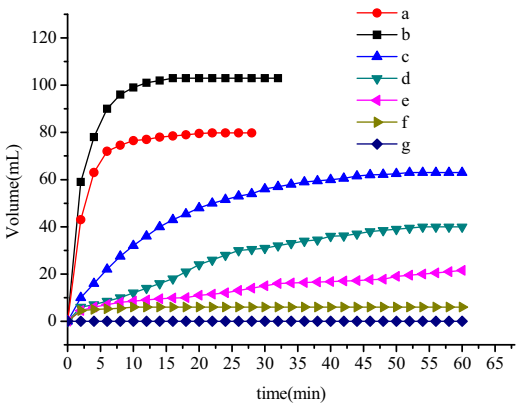

Fig. 1. Gas generation by decomposition of FA/SF with different ratios of Ag/Pd supported on ZIF-8 versus time (a) Pd@ZIF-8, (b) $Ag_{18}Pd_{82}$@ZIF-8, (c) $Ag_{36}Pd_{64}$@ZIF-8, (d) $Ag_{48}Pd_{52}$@ZIF-8, (e) $Ag_{58}Pd_{42}$@ZIF-8, (f) $Ag_{76}Pd_{24}$@ZIF-8, (g) Ag@ZIF-8 at 353 K. (n_{FA} = 3 mmol, n_{SF} = 1 mmol).

Quantachrome NOVA 4200e. The inductively coupled plasma-atomic emission spectroscopy (ICP-AES) was performed on IRIS Intrepid II XSP (Thermo Fisher Scientific, USA). Detailed analyses for CO_2, H_2 and CO were performed on GC-9790 (Zhejiang Fuli Analytical Instrument CO., Ltd.) with thermal conductivity detector (TCD) flame ionization detector (FID)-Methanator (detection limit: ~10 ppm). A standard gas sample consist of 20.4% CO_2, 0.005% CO, 59.69% N_2, 19.9% H_2 was used to calibrate the GC. The H_2 and CO_2 compositions were measured by GC spectrum using TCD, while CO was measured by GC spectrum using FID-Methanator.

3. Results and discussions

ZIF-8 was synthesized according to the literature [34]. AgPd@ZIF-8 catalysts were prepared through solution infiltration of activated ZIF-8 with H_2PdCl_4 and $AgNO_3$ at 298 K, followed by treatment with $NaBH_4$ at 273 K. The composition of the AgPd NPs was tuned by the initial molar ratio of H_2PdCl_4 and $AgNO_3$, and further determined by inductively coupled plasma-atomic emission spectroscopy (ICP-AES) as shown in Table S1. The Pd@ZIF-8, $Ag_{18}Pd_{82}$@ZIF-8, $Ag_{36}Pd_{64}$@ZIF-8, $Ag_{48}Pd_{52}$@ZIF-8, $Ag_{58}Pd_{42}$@ZIF-8, $Ag_{76}Pd_{24}$@ZIF-8, Ag@ZIF-8 were synthesized using metal precursors at the Ag/Pd ratios of 0:5, 1:4, 2:3, 1:1, 3:2, 4:1, 5:0, respectively. The catalytic dehydrogenation of FA has been performed over all the samples at 353 K in the presence of sodium formate (HCOONa, SF) as shown in Fig. 1, Table S2. Catalytic performances of all the catalysts were studied based on the amount of gases measured volumetrically during the reaction. Their catalytic activities were strongly depended on the composition of AgPd clusters. The Ag@ZIF-8 was almost catalytic inactive, while by alloying Pd and increasing the composition of Pd, the catalytic activity increased accordingly, and $Ag_{18}Pd_{82}$@ZIF-8 exhibits extremely high catalytic activity with the turnover frequency (TOF) value of 580 h^{-1} at 80 °C, which is among the highest value of the previously reported catalysts (Table 1). Further increasing the Pd composition to pure Pd@ZIF-8 resulted in the decrease in catalytic activity, highlighting the synergistic effect of molecular-scale AgPd alloy composition in ZIF-8 for the catalytic dehydrogenation of FA. Furthermore, as a control experiment, the same amount of $Ag_{18}Pd_{82}$ NPs immobilized on different supports were synthesized and applied to the same catalytic reaction (Fig. S1). Almost no reactivity was observed for ZIF-8, and less than 30 mL gas was generated over 20 min for $Ag_{18}Pd_{82}$ NPs, indicating the synergetic effect of AgPd and ZIF-8. Additionally, to study the effects of supported materials on the catalytic performances of the as-synthesized catalysts, free $Ag_{18}Pd_{82}$ NPs and $Ag_{18}Pd_{82}$ NPs supported on C, SiO_2 and Al_2O_3 were synthesized, and their catalytic activity toward dehydrogenation of FA were shown in Fig. S1. Among all the catalysts tested, $Ag_{18}Pd_{82}$@ZIF-8 exhibits the highest catalytic performance, which further demonstrates synergetic effect of AgPd and ZIF-8.

Table 1
Comparison of activities of different catalysts for hydrogen generation from FA/SF.

Catalyst	T (K)	TOF (h^{-1})	E_a (kJ/mol)	Reference
$Ag_{18}Pd_{82}$@ZIF-8	353	580	51.38	This work
Pd-Au-Eu/C	365	387	84.2	[28]
Ag@Pd	293	125	30.0	[30]
Ag/Pd alloy	293	144	30	[30]
Monodisperse $Ag_{42}Pd_{58}$/C	323	382	22	[32]
$Ni_{18}Ag_{24}Pd_{58}$/C	323	85	20.5	[27]
Pd/C	323	30		[33]
Monodisperse $Au_{41}Pd_{59}$/C	323	230	28	[33]
Pd-Au/C	365	45	138.6	[45]
Pd/C with citric acid	298	64		[46]
AuPd@ED-MIL-101	363	106		[34]
$PtRuBiO_x$/C	353	312	37.3	[47]
PdNi/GN_S-CB	298	529		[22]
PdAu/C-CeO_2	365	113.5		[45]
$Co_{0.30}Au_{0.35}Pd_{0.35}$	298	80		[29]
Pd-S-SiO_2	358	719		[48]
Au/C	323	80		[33]

$TOF_{initial}$ were calculated during the first 5 min of the reactions.

It is known that the molar ratio of FA/SF has a great effect on the catalytic activity of nanocatalysts. In order to explore the best molar ratio of FA and SF in our system, we studied the hydrogen generation from FA/SF solution with different FA/SF molar ratios over $Ag_{18}Pd_{82}$@ZIF-8 at 80 °C (Fig. 2). Without SF, less than 30 mL gas was released, while increasing the amount of SF to the molar ratio of 3:1 (FA/SF), the catalyst exhibits highest catalytic activity. Further increasing the amount of SF resulted in the decrease of activity of $Ag_{18}Pd_{82}$@ZIF-8. Moreover, without FA, no gas was generated from pure SF solution.

The gas generated from the reaction was passed through a trap containing 5 M NaOH solution to ensure the complete absorption of CO_2 (Fig. S2). The volume of gas after passing through NaOH trap was reduced to half, indicating generation of hydrogen and carbon dioxide completely, with no evidence of CO. Furthermore, only CO_2 but no CO has been detected by gas chromatography (GC) analyses (Figs. S3 and S4), indicating the excellent H_2 selectivity for formic acid dehydrogenation by $Ag_{18}Pd_{82}$@ZIF-8 catalyst.

To get the activation energy (E_a) of the dehydrogenation of FA catalyzed by $Ag_{18}Pd_{82}$@ZIF-8, the dehydrogenation reactions at different temperature ranging from 50 to 80 °C were carried out. The values of rate constant k at different temperatures were calculated from the slope of the linear part of each plot from

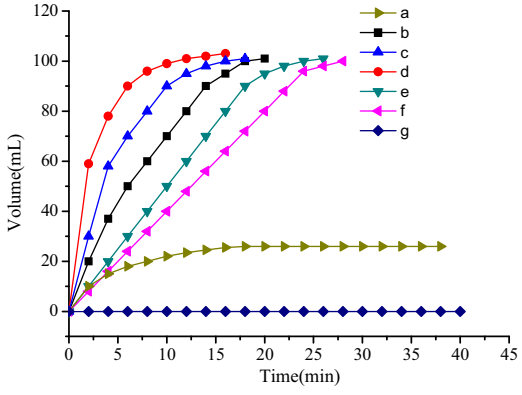

Fig. 2. Gas generation by decomposition of FA/SF with different FA/SF molar ratios (a) 18:0 (b) 18:2 (c) 18:3 (d) 18:6 (e) 18:9 (f) 18:12 (g) 0:18 versus time catalyzed by $Ag_{18}Pd_{82}$@ZIF-8 at 353 K. (n_{FA} = 3 mmol).

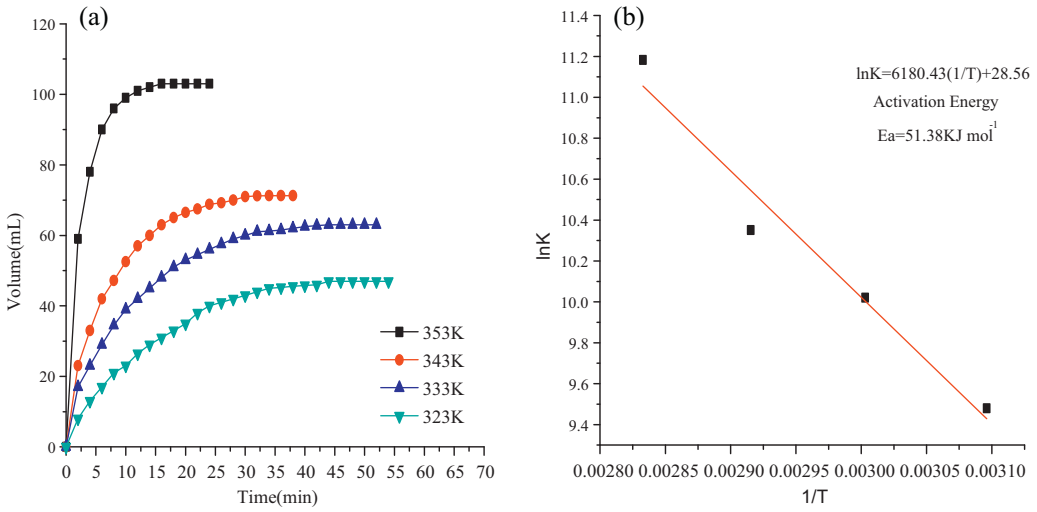

Fig. 3. (a) Time course plots for hydrogen generation by the decomposition of FA/SF by $Ag_{18}Pd_{82}$@ZIF-8 at 323 K, 333 K, 343 K and 353 K. (b) Plot of ln k versus $1/T$ during the FA/SF decomposition over $Ag_{18}Pd_{82}$@ZIF-8 at different temperatures. (n_{FA} = 3 mmol, n_{SF} = 1 mmol).

Fig. 3a. The Arrhenius plot of ln k versus $1/T$ for the catalyst is plotted in Fig. 3b, from which the apparent activation energy was determined to be approximately 51.38 kJ/mol, which is lower than most reported values (Table 1).

Furthermore, we tested the recyclability of the $Ag_{18}Pd_{82}$@ZIF-8 catalyst in the dehydrogenation of FA/SF at 80 °C (Fig. S5). It showed that the as-synthesized catalysts still exhibit certain catalytic activity without no decrease in the hydrogen selectivity even after the fifth run. After the recyclability experiment, the resulting solution was filtered and 95% AgPd still remain in the catalyst as confirmed by ICP-AES. In addition, the integrity of the ZIF-8 framework is maintained well, as indicated in PXRD (*vide infra*). TEM images of $Ag_{18}Pd_{82}$@ZIF-8 catalyst after the recyclability experiment show that the AgPd NPs aggregate on ZIF-8 (*vide infra*).

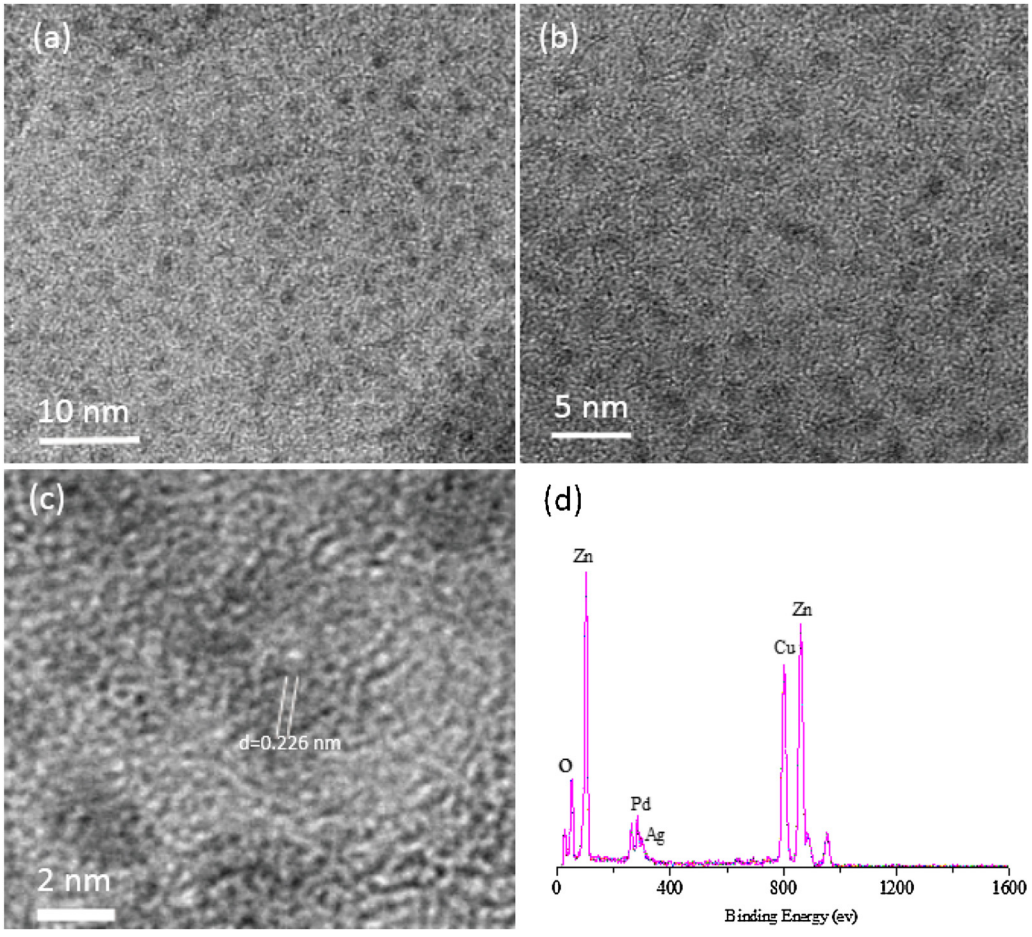

Fig. 4. (a–c) TEM images of $Ag_{18}Pd_{82}$@ZIF-8 with different magnifications. (d) EDX spectrum of Ag18Pd82@ZIF-8.

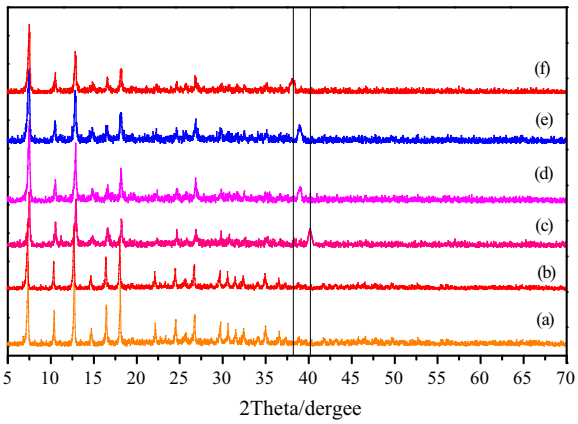

Fig. 5. Powder X-ray diffraction patterns for (a) the as-prepared ZIF-8, (b) activated ZIF-8, (c) Ag@ZIF-8, (d) $Ag_{18}Pd_{82}$@ZIF-8, (e) $Ag_{18}Pd_{82}$@ZIF-8 after five cycles of catalysis, (f) Pd@ZIF-8. The characteristic peak of Pd (1 1 1) is at $2\theta = 40.1^\circ$, the characteristic peak of Ag (1 1 1) is at $2\theta = 38.03^\circ$.

Therefore, the decrease of catalytic activity can be attributed to the aggregation of AgPd NPs. Further work about enhancement of the recyclability of the as-synthesized catalyst for dehydrogenation of FA is underway.

The morphologies of ZIF-8 immobilized $Ag_{18}Pd_{82}$ NPs were characterized by transmission electron microscopic (TEM) and energy-dispersive X-ray spectroscopy (EDX) measurements (Fig. 4). TEM images of AgPd@ZIF-8 indicate that the AgPd NPs with a mean diameter of 1.6 ± 0.2 nm (Fig. S6) were well dispersed, and encapsulated in the cages of the ZIF-8, which may explain the high catalytic activity for dehydrogenation of formic acid. A representative high-resolution TEM image in Fig. 4c shows the *d*-spacing of 0.226 nm, which is between the (1 1 1) lattice spacing of face-centered cubic (*fcc*) Ag (0.24 nm) and *fcc* Pd (0.22 nm), suggesting that AgPd is formed as an alloy structure. For comparison, the TEM images of pure ZIF-8 and $Ag_{18}Pd_{82}$@ZIF-8 after recyclability experiment were shown in Figs. S7 and S8. The EDX spectra (Fig. 4d) further confirm the presence of AgPd. The powder X-ray diffractions (PXRD) of the as-synthesized ZIF-8, activated ZIF-8, Pd@ZIF-8, Ag@ZIF-8, $Ag_{18}Pd_{82}$@ZIF-8, and $Ag_{18}Pd_{82}$@ZIF-8 after the stability test exhibit no loss of crystallinity (Fig. 5), indicating that the integrity of the ZIF-8 framework is maintained well during the catalyst preparation and catalytic process. Furthermore, the PXRD pattern of $Ag_{18}Pd_{82}$@ZIF-8 exhibited a well-defined diffraction peak between the characteristic peaks of Ag (1 1 1) and Pd (1 1 1), indicating the formation of the AgPd alloy. The N_2 adsorption–desorption isotherms of ZIF-8, $Ag_{76}Pd_{24}$@ZIF-8, $Ag_{58}Pd_{42}$@ZIF-8, $Ag_{48}Pd_{52}$@ZIF-8, $Ag_{36}Pd_{64}$@ZIF-8, and $Ag_{18}Pd_{82}$@ZIF-8 were shown in Fig. S9. The large decrease in the amount of N_2 adsorption and the pore volume (Table S2) of AgPd@ ZIF-8 indicates that the cavities of ZIF-8 were either occupied or blocked by the well dispersed AgPd NPs [41,42]. In the X-ray photoelectron spectroscopy (XPS) (Fig. S10), the $3d^{5/2}$ and $3d^{3/2}$ peaks of Pd^0 appear at 336.2 and 342.4 eV [43], and the $3d^{5/2}$ and $3d^{3/2}$ peaks of Ag^0 appear at 373.8 and 367.0 eV, with no obvious peak of Ag^+ and Pd^{2+} observed [44], indicating the co-existence of both metals.

In conclusion, we have developed a highly efficient heterogeneous catalyst system in dehydrogenation of formic acid for chemical hydrogen storage using ZIF-8 supported AgPd NPs as the catalysts. For the first time, the synergistic effect of AgPd composition in MOFs for the catalytic dehydrogenation of formic acid was studied. The $Ag_{18}Pd_{82}$@ZIF-8 catalyst exhibits a marked superiority over the monometallic and other bimetallic counterparts with different composition, indicating a strong molecular-scale synergy of Ag–Pd alloy. The combination of high activity and selectivity, as well as good durability may further promote the practical application of formic acid as a hydrogen storage material in the "hydrogen economy".

Acknowledgments

This work was financially supported by the National Natural Science Foundation of China (21201134), the Natural Science Foundation of Jiangsu Province (BK20130370), the Natural Science Foundation of Hubei Province (2013CFB288), the Creative Research Groups of Hubei Province (2014CFA007) and Large-scale Instrument and Equipment Sharing Foundation of Wuhan University.

Appendix A. Supplementary data

Supplementary data associated with this article can be found, in the online version, at http://dx.doi.org/10.1016/j.apcatb.2014.09.065.

References

[1] C. Wang, D. Liu, W. Lin, J. Am. Chem. Soc. 135 (2013) 13222–13234.
[2] R.C. Huxford, J. Della Rocca, W.-B. Lin, Curr. Opin. Chem. Biol. 14 (2010) 262–268.
[3] F.A. Almeida Paz, J. Klinowski, S.M.F. Vilela, J.P.C. Tome, J.A.S. Cavaleiro, J. Rocha, Chem. Soc. Rev. 41 (2012) 1088–1110.
[4] D. Zhao, D.J. Timmons, D. Yuan, H.-C. Zhou, Acc. Chem. Res. 44 (2011) 123–133.
[5] Q. Yang, D. Liu, C. Zhong, J.-R. Li, Chem. Rev. 113 (2013) 8261–8323.
[6] S.H. Jhung, N.A. Khan, Z. Hasan, CrystEngComm 14 (2012) 7099–7109.
[7] Z.-Y. Gu, C.-X. Yang, N. Chang, X.-P. Yan, Acc. Chem. Res. 45 (2012) 734–745.
[8] D. Bradshaw, A. Garai, J. Huo, Chem. Soc. Rev. 41 (2012) 2344–2381.
[9] A. Aijaz, T. Akita, N. Tsumori, Q. Xu, J. Am. Chem. Soc. 135 (2013) 16356–16359.
[10] S. Pullen, H. Fei, A. Orthaber, S.M. Cohen, S. Ott, J. Am. Chem. Soc. 135 (2013) 16997–17003.
[11] M.S. El-Shall, V. Abdelsayed, A.E.R.S. Khder, H.M.A. Hassan, H.M. El-Kaderi, T.E. Reich, J. Mater. Chem. 19 (2009) 7625–7631.
[12] P.-Z. Li, K. Aranishi, Q. Xu, Chem. Commun. 48 (2012) 3173–3175.
[13] C.-H. Kuo, Y. Tang, L.-Y. Chou, B.T. Sneed, C.N. Brodsky, Z. Zhao, C.-K. Tsung, J. Am. Chem. Soc. 134 (2012) 14345–14348.
[14] H.L. Jiang, T. Akita, T. Ishida, M. Haruta, Q. Xu, J. Am. Chem. Soc. 133 (2011) 1304–1306.
[15] H.-L. Jiang, S.K. Singh, J.-M. Yan, X.-B. Zhang, Q. Xu, ChemSusChem 3 (2010) 541–549.
[16] K.M.K. Yu, I. Curcic, J. Gabriel, S.C.E. Tsang, ChemSusChem 1 (2008) 893–899.
[17] W. Grochala, P.P. Edwards, Chem. Rev. 104 (2004) 1283–1316.
[18] J. Graetz, Chem. Soc. Rev. 38 (2009) 73–82.
[19] M.P. Suh, H.J. Park, T.K. Prasad, D.-W. Lim, Chem. Rev. 112 (2011) 782–835.
[20] A. Staubitz, A.P.M. Robertson, I. Manners, Chem. Rev. 110 (2010) 4079–4124.
[21] Q.-L. Zhu, N. Tsumori, Q. Xu, Chem. Sci. 5 (2014) 195–199.
[22] Y.L. Qin, J. Wang, F.Z. Meng, L.M. Wang, X.B. Zhang, Chem. Commun. 49 (2013) 10028–10030.
[23] M. Martis, K. Mori, K. Fujiwara, W.-S. Ahn, H. Yamashita, J. Phys. Chem. C 117 (2013) 22805–22810.
[24] M. Grasemann, G. Laurenczy, Energy Environ. Sci. 5 (2012) 8171–8181.
[25] Y. Ping, J.-M. Yan, Z.-L. Wang, H.-L. Wang, Q. Jiang, J. Mater. Chem. A 1 (2013) 12188–12191.
[26] K. Mori, M. Dojo, H. Yamashita, ACS Catal. 3 (2013) 1114–1119.
[27] M. Yurderi, A. Bulut, M. Zahmakiran, M. Kaya, Appl. Catal. B 160–161 (2014) 514–524.
[28] X. Zhou, Y. Huang, C. Liu, J. Liao, T. Lu, W. Xing, ChemSusChem 3 (2010) 1379–1382.
[29] Z.-L. Wang, J.-M. Yan, Y. Ping, H.-L. Wang, W.-T. Zheng, Q. Jiang, Angew. Chem., Int. Ed. 52 (2013) 4406–4409.
[30] K. Tedsree, T. Li, S. Jones, C.W.A. Chan, K.M.K. Yu, P.A.J. Bagot, E.A. Marquis, G.D.W. Smith, S.C.E. Tsang, Nat. Nanotechnol. 6 (2011) 302–307.
[31] Z.-L. Wang, J.-M. Yan, H.-L. Wang, Y. Ping, Q. Jiang, J. Mater. Chem. A 1 (2013) 12721–12725.
[32] S. Zhang, O. Metin, D. Su, S. Sun, Angew. Chem., Int. Ed. 52 (2013) 3681–3684.
[33] O. Metin, X. Sun, S. Sun, Nanoscale 5 (2013) 910–912.
[34] X. Gu, Z.-H. Lu, H.-L. Jiang, T. Akita, Q. Xu, J. Am. Chem. Soc. 133 (2011) 11822–11825.
[35] B. Xia, N. Cao, H. Dai, J. Su, X. Wu, W. Luo, G. Cheng, ChemCatChem 6 (2014) 2549–2552.
[36] M. Zahmakiran, Dalton Trans. 41 (2012) 12690–12696.
[37] M. Yurderi, A. Bulut, M. Zahmakiran, M. Gulcan, S. Ozkar, Appl. Catal. B 160–161 (2014) 534–541.
[38] A.K. Singh, Q. Xu, ChemCatChem 5 (2013) 3000–3004.
[39] K.S. Park, Z. Ni, A.P. Côté, J.Y. Choi, R. Huang, F.J. Uribe-Romo, H.K. Chae, M. O'Keeffe, O.M. Yaghi, Proc. Natl. Acad. Sci. 103 (2006) 10186–10191.

[40] O. Karagiaridi, M.B. Lalonde, W. Bury, A.A. Sarjeant, O.K. Farha, J.T. Hupp, J. Am. Chem. Soc. 134 (2012) 18790–18796.
[41] G. Chen, S. Wu, H. Liu, H. Jiang, Y. Li, Green Chem. 15 (2013) 230–235.
[42] Y. Huang, S. Liu, Z. Lin, W. Li, X. Li, R. Cao, J. Catal. 292 (2012) 111–117.
[43] H. Dai, J. Su, K. Hu, W. Luo, G. Cheng, Int. J. Hydrogen Energy 39 (2014) 4947–4953.
[44] L. Yang, W. Luo, G. Cheng, ACS Appl. Mater. Interfaces 5 (2013) 8231–8240.
[45] X. Zhou, Y. Huang, W. Xing, C. Liu, J. Liao, T. Lu, Chem. Commun. (2008) 3540–3542.
[46] A.K. Singh, M. Yadav, K. Aranishi, Q. Xu, Int. J. Hydrogen Energy 37 (2012) 18915–18919.
[47] S.-W. Ting, S. Cheng, K.-Y. Tsang, N. van der Laak, K.-Y. Chan, Chem. Commun. (2009) 7333–7335.
[48] Y. Zhao, L. Deng, S.-Y. Tang, D.-M. Lai, B. Liao, Y. Fu, Q.-X. Guo, Energy Fuels 25 (2011) 3693–3697.